

Phase transitions in ensembles of solitons induced by an optical pumping or a strong electric field.

P. Karpov¹ and S. Brazovskii^{1,2}

¹*National University of Science and Technology "MISiS", Moscow, 119049, Russia*

²*CNRS UMR 8626 LPTMS, Univ. Paris-Sud, Univ. Paris-Saclay, Orsay, France*

(Dated: May 10, 2016)

The latest trend in studies of modern electronically and/or optically active materials is to provoke phase transformations induced by high electric fields (the electrostatic doping) and by short (femtosecond) powerful optical pulses. The accessed cooperative electronic states include superconductivity, anti-ferromagnetism, ferroelectricity, charge order, charge- and spin density waves, Mott and Peierls insulators. Vulnerabilities of the broken symmetries give rise to topological defects like electronic vortices, walls, stripes. The typical low-dimensional architecture of these compounds brings these objects to a microscopic scale giving rise to solitons: self-localized configurations which shapes explore the ground state degeneracy. The solitons can be the lowest energy optical excitations or the carriers of charge or/and spins, taking these functions from conventional electrons. Their new identifications and even direct visualizations were a true experimental success of recent years. Because of the long-range ordering, the solitons experience unusual super long-range forces which lead to a sequence of phase transitions in their ensembles: the higher temperature transition of the confinement and the lower one of aggregation into macroscopic walls. Here we perform an intensive numerical modeling for ensembles of both neutral and charged solitons in three- and two-dimensional systems. We suggest a specific Monte Carlo algorithm preserving the number of solitons which substantially simplifies the calculations, allows to extend them to the three-dimensional case and to include long-range Coulomb interactions. The results confirm the confinement transition, except for a very strong Coulomb repulsion, and demonstrate the patterns formation at the second transition of aggregation. Beyond possible applications to modern experiments in electronic systems, the modeling of the cooperative confinement transition touches also not yet resolved questions in high energy physics and cosmology.

PACS numbers: 03.75.Lm 05.45.Yv 05.50.+q 05.70.Fh 64.60.Cn 68.35.Rh 89.75.Kd

Keywords: topological defect, soliton, kink, stripe, confinement, aggregation, PIPT, optical pumping, electrostatic doping

I. INTRODUCTION.

A. Solitons via doping or pumping.

A new trend in controlling cooperative states of interacting electronic systems is applying either very short (10's of femtoseconds) powerful optical pulses or very high (up to 10^7 V/cm) electric fields, see¹⁻⁶. These impacts result in a very high (up to 10% per lattice site) concentration of excitations and/or charge carriers. There are convincing arguments that these states will not resemble ensembles of electrons and/or holes like for optical pumping or field-effect injection in conventional semiconductors. The reason is that commonly the exploited strongly correlated electronic systems show various types of symmetry breaking giving rise to degenerate ground states. The degeneracy allows for topologically nontrivial configurations exploring the possibility of traveling through different allowed ground states. Their most known forms are plain domain walls, vortex lines or dislocations, which are still macroscopic objects extending in one or two dimensions. Most importantly, there are also totally localized and truly microscopic objects which energies and quantum numbers are on the one-electron scale. These anomalous particles – the solitons – can determine the observable properties, which are usually

ascribed to conventional electronic excitations, see^{7,8} for early theory reviews and⁹⁻¹¹ for updates.

The fact that the solitons have quantum eigenvalues (charge or spin) makes it possible to monitor their concentration. The electrostatic doping (see the review⁴ and updates in^{5,6}) should give rise to the stable $2D$ ensemble of similarly charged kinks in a thin, sometimes atomically narrow, surface layer. The optical pumping should give rise firstly to the equal number of oppositely charged solitons which collisions will work to convert them secondly to the ensemble of neutral spin-carrying solitons (which usually have lower energy than the charged ones¹²). Inevitably, the recombination will follow, may be via formation of excitons as pairs of oppositely charged kinks¹³. But the optical emission will take long (more than nanoseconds) time which can be further prolonged by the intermediate conversion to neutral spin-carrying solitons which can recombine only via triplet channels – the effect is well documented in optics of conducting polymers^{12,14}. Then for a typically very fast pump-induced phase transition experiments even the system of oppositely charged solitons, and even more of spin-carrying ones, can be treated as quasi-stationary, with only slowly decreasing number of particles. This number is exactly conserved and monitored in experiments with the electrostatic doping.

Such ensembles of solitons are expected to have a peculiar phase diagram, with several lines of phase transitions which are inevitably crossed in the course of the evolution or monitoring the concentration and the temperature. Study of these transitions is the main goal of this article. In the next section of the Introduction we shall summarize modern experimental and theoretical evidences in favor of existence of solitons in electronic systems. In Ch.II we shall give a qualitative picture of phase transitions in ensembles of neutral and charged solitons. The central issue is the confinement interaction specific to solitons in contrast to conventional electrons. In Ch.III we shall introduce the basic model, which is mapped onto the Ising model, and also present some analytical results. In Ch.IV we shall present new results of extensive numerical modeling, which was challenging for three-dimensional systems, particularly in presence of Coulomb interactions (CI). We shall observe a high temperature transition of confinement of solitons into pairs and particularly rich and interesting low temperature transition of solitons aggregation into domain walls transversing the sample. Ch.V is devoted to discussion and summary. The Appendix contains estimations for aggregation of neutral and charged solitons.

B. New accesses to microscopic solitons in quasi one-dimensional electronic systems.

There are growing experimental evidences on existence of microscopic solitons and their determining role in electronic processes of quasi-1D systems: conjugated polymers (see⁸ on theory and¹⁵ on experiment), spin-Peierls chains¹⁶, donor-acceptor stacks including "electronic ferroelectrics"^{17,18}, and families of so called "electronic crystals": charge density waves (CDW) and charge-ordered Mott insulators (see reviews^{9,10,19}). Solitons take over band electrons in roles of primary excitations – charge or spin carriers, since their activation energies are typically lower than gaps opened in the electronic spectra. The solitons feature self-trapping of electrons into mid-gap states and separation of spin and charge into spinons and holons, sometimes with their reconfinement at essentially different scales. Thus, the ferroelectric charge ordering in organic conductors (see a review¹⁹) gives access to several types of solitons observed in conductivity (holons) and in permittivity (polar kinks), to solitons' bound pairs in optics, to compound charge-spin solitons. In CDWs²⁰ and in surface nano-wires²¹ the individual solitons, which are the amplitude kinks, have been visually captured in STM experiments; this is the most remarkable new achievement in proving the existence of solitons. The resolved subgap tunneling spectra²² recover presumably the same solitons in dynamics. The tunneling creation of solitons' pairs describes nonlinear transport in CDWs²³ and polymers^{24,25}. The solitons can be also viewed as nucleus of the melted stripe phase in doped Mott insulators or of the FFLO phase in spin polarized

superconductors^{26,27}.

On this basis one can extrapolate to a picture of combined topological excitations in general strongly correlated systems: from doped antiferromagnets to strong-coupling and spin-polarized superconductors¹⁰.

II. INTERACTIONS AND PHASE TRANSITIONS IN ENSEMBLES OF SOLITONS.

A. Interactions of solitons

Following the above quoted experimental confirmations and theoretical results, we shall consider a system where the solitons serve as the lowest (with respect to band electrons) energy forms of storage of the charge or the spin. We shall restrict the study to the case of a discrete symmetry breaking, which is a very common phenomenon of a dimerization of bonds (the family of Peierls-like transitions) or of sites (the family of transitions with charge ordering or disproportionation). Cases of continuous symmetries like incommensurate CDWs, spin density waves and superconductors, require for a special consideration. Such a system possesses typically three types of solitons: spinless with charges $\pm e$ and a neutral with the spin $1/2$. In ferroelectric systems (see a recent review²⁸) all solitons should carry non-integer charges. With passing of such a soliton, the order parameter changes the sign, hence the nickname "the amplitude kink", or just the kink or the soliton which we shall use in the following.

The solitons are subject to all kind of interactions, among themselves and also with the lattice, known for conventional electrons. The important CI can or cannot be screened by external carriers depending on the nature of the gate of the field-effect transistor, and we shall consider both cases. But beyond that, there is the unusual super long-range interaction specific to the solitons as topologically nontrivial objects. The soliton is a 1D domain boundary, which interrupts the proper interchain arrangement. That gives rise to the confinement energy Fl_{bs} , with the constant confinement force F , growing linearly with the distance between solitons l_{bs} – see Figs.1-3. This energy dominates at long distances even if it can be unimportant locally for a crystal of weakly interacting chains.

In some special cases, the ground state degeneracy can be lifted by an internal effect globally – for the whole system. The bright example is the cis-polyacetylene^{7,13,15}, where the solitons are always confined in pairs. In cases of continuous symmetries, the ordering violated by the amplitude kink can be restored by changes in the phase of the order parameter $\Psi(x)$, localized in the tails of a soliton of length $l_{phase} \sim T_c^{-1}$, where T_c is the temperature of the long-range ordering due to the interchain coupling. But universally, except truly 1D systems like isolated atomic chains²¹, there is a local lifting of degeneracy which comes from interchain interactions – their parts

which are responsible for establishing the long-range $2D$ or $3D$ ordering. Namely, the interchain ordering energy J_{\perp} (per lattice unit of the length a_{\parallel}) is paid when adjacent domains at neighboring chains are not rightly correlated.

The confinement interaction determines the intermediate phases and the kinetics of aggregation of non-equilibrium (e.g. optically induced) domains into the long-range ordered phase.

B. Qualitative description of phase transitions in the ensemble of neutral solitons

Consider the influence of weak ordering interaction between chains ($2D$ or $3D$ coupling) on the state and statistical properties of the kink-like solitons²⁹. The weak interchain coupling does not affect substantially the structure of the soliton core, but below the $2D$ or $3D$ ordering temperature T_1 its role turns out to be fundamental at large distances x . Since each kink separates different states of the system, the correlation between the chains is violated in its vicinity. As a result, the system loses an energy $2J_{\perp}$ per site, which increases proportionally to the distance x from the soliton. As we see from Figs.1-3 the energy grows both with separation of two solitons on one chain and among solitons at neighboring chains, hence the tendencies to either formation of on-chain bikinks or the interchain aggregation of solitons into walls. As a result of these contradictory tendencies, as temperature lowers, the system passes through two phase transitions: the coupling of solitons into pairs at $T = T_1$, and aggregation of pairs between the chains at lower $T = T_2 \ll T_1$. For a three-dimensional system, the temperature T_2 is a phase-transition point, below which plane domain walls appear in the system passing through the entire cross section. For a two-dimensional system, there is no distinct second transition, but a gradual increase of the transverse dimension of the paired walls takes place at $T < T_2$. For a finite system, like in our modeling, there is a sample dependent temperature T_F where the first wall crosses the whole sample even in $D = 2$.

This qualitative picture is based upon an exact solution available for a $2D$ system of neutral solitons with some qualitative extensions to the $3D$ case²⁹. The case of charged solitons has been addressed in³¹, but only for the $2D$ case and with a restrictive constraint: the bisoliton pairs were not supposed to move from one chain to another. Here we shall present results of unrestricted numerical modeling performed for the challenging case of a $3D$ system, both for neutral and charged ensembles of solitons.

In short, the picture of equilibrium states is the following. With lowering T at a given concentration of kinks ν , the system passes through a sequence of two phase transitions (at $T = T_1, T_2$) and a crossover (at $T = J_{\perp}$), which are determined by three scales of energy: J_{\perp} as the local energy of the interchain ordering of spins, the

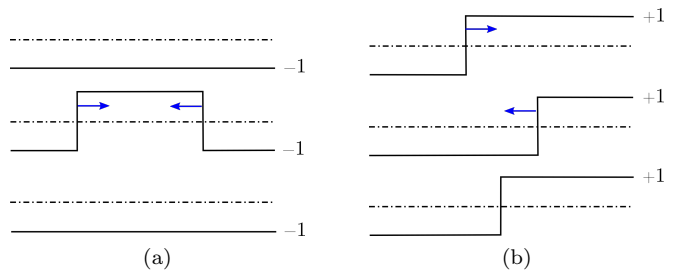


FIG. 1: (Color online) High temperature $T > T_1$: Solitons exist as individual entities. They already experience long-range attraction towards binding them into pairs at the same chain (a) or to walls at neighboring chains (b). Horizontal black lines correspond to ground states with the order parameter ± 1 , vertical lines represent kinks, arrows show forces acting upon the kinks.

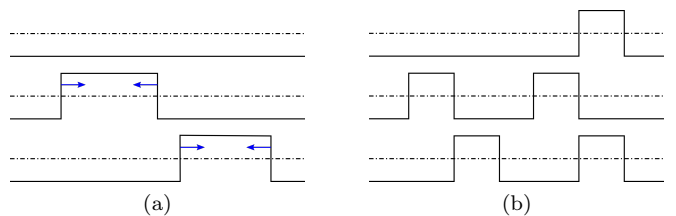


FIG. 2: (Color online) Intermediate temperatures within $T_1 > T > T_2$. There are no more individual solitons, but a gas of their confined pairs. The pairs lengths are loose and fluctuate at $T_1 > T > J_{\perp}$ (a); they are tight at $J_{\perp} > T > T_2$ (b).

bigger $T_1 \propto J_{\perp}/\nu$ as the nonlocal energy of solitons' confinement, and the smaller $T_2 \propto J_{\perp}/\ln(1/\nu)$ as the characteristic energy of solitons' transverse aggregation.

I. $T_1 \propto Fl \propto J_{\perp}/\nu$ (see Figs.1,2) is the conventional $3D$ ordering transition in realities of a quasi- $1D$ system. But for the ensemble of solitons, this is the confinement transition, which takes place when the temperature decreases below the mean interchain interaction Fl at the mean distance $l = a_{\parallel}/\nu$ between the solitons. Below that, at $T < T_1$, individual on-chain solitons cannot exist, they are confined into loose pairs which form strings of size l_{bs} with the energy Fl_{bs} among them (T_1 can be also defined by the condition $l_{bs} \sim l$, when confined pairs dissociate).

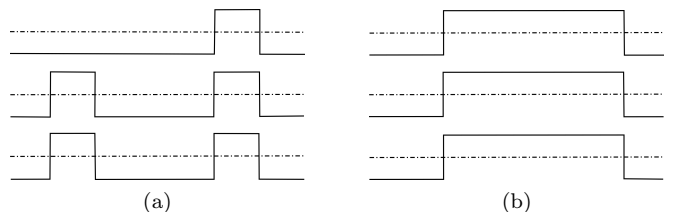


FIG. 3: Low temperatures $T < T_2$: aggregation of pairs into growing bikink walls (a) and then their disintegration into isolated walls of kinks (b).

With lowering T , the pairs become progressively more confined at the thermal length $l_T = T/F \ll l$, with rare collisions among the pairs. The confinement energy is reduced from the high- T scale J_\perp per unit cell to J_\perp per kinks' pair. At $T \ll J_\perp$, the pairs become tightly bound, their spacing does not fluctuate anymore. Actually, the pair length l_{bs} shrinks from the thermal one l_T to the quantum zero point limit l_q where $Fl_q \sim \hbar^2/Ml_q^2$ (M is an effective mass of the soliton).

Thus, the energy T_1 serves two functions. For spins, this is just the transition temperature $T_1 = T_c$ for the second order phase transition to the state with a nonzero mean spin value $m = \langle S_{n,\alpha} \rangle \neq 0$ at $T < T_c$. But for solitons this is the confinement transition, below which they become bound into pairs – the bisolitons.

II. $T_2 \propto J_\perp / \ln(1/\nu) < J_\perp$ (see Fig.3) is the temperature which can be viewed as the aggregation of solitons temperature when first domain walls appear crossing the whole sample or forming macroscopic bubbles. As the temperature lowers from J_\perp , the bisolitons start to aggregate in transverse disks, and finally at T_2 these disks cross the entire sample. Aggregation to domain walls gains the confinement energy which now is not lost at all – the neighboring chains are always in the right arrangement. But the entropy is lost, and this balance determines T_2 . The pairs still coexist with walls below T_2 , but with further decreasing T they vanish providing the material for building more of macroscopic walls.

The T_2 transition can be viewed similarly to a vapor condensation in a given volume when the first appearing wetting fixes the chemical potential (the saturation pressure) of the gas. Another analogy is the Bose-Einstein condensation, but in real, instead of the reciprocal, space. Indeed, below J_\perp , there is the gas of "confined pairs" (bisolitons) with the energy $W_{bs} = Fl_{T,q}$ which chemical potential μ_{bs} is adjusted to maintain the given total $n_{bs}(\mu_{bs}, T) = \exp((\mu_{bs} - W_{bs})/T) = \nu/2$. When the first macroscopic domain walls appear, they serve as a reservoir of kinks fixing their chemical potential – ideally at $\mu_s = 0$, hence $\mu_{bs} = 2\mu_s = 0$. Then the number of pairs is $\nu_{bs}(0, T) = \exp(-W_{bs}/T)$, and this number falls below the total available $\nu_{bs} = \nu/2$, which happens at $T < T_2$. The deficit $\delta\nu = \nu - \nu_{bs}(0, T)$ gives the number of solitons that have been used to build the domain walls, with $a_{||}/\delta\nu$ giving the mean period of the stripe array of domain walls. Notice a curious behavior: with lowering T below T_2 , the mean value of the order parameter over the bulk disappears, while it is present over each cross-section. The T_2 transition is the one where the effective dimensionality of the system D is reduced by 1! We shall see this explicitly via the effective Ising model with constraints.

C. Evolution after the optical pumping.

After the optical pulse has created the ensemble of solitons, their mean concentration ν starts to evolve as $\nu(t)$

both to thermal equilibrium at a given T and also together with the temperature $T(t)$. On this way, the system will pass through a sequence of phase transitions or at least of crossovers among different regimes which have been classified above. The trajectory is summarized in Fig.4.

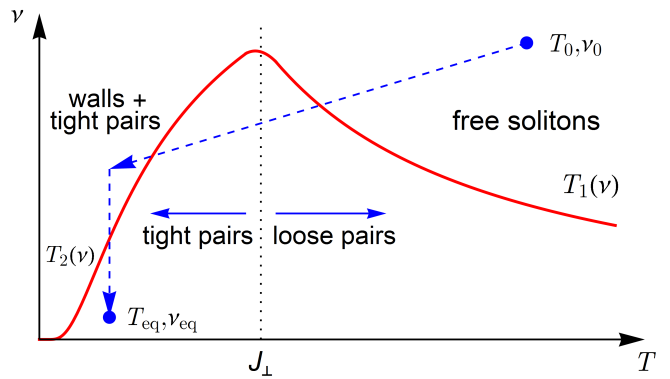


FIG. 4: (Color online) The phase diagram of the solitons' ensemble in variables $T - \nu$. Thick solid lines show the phase transitions T_1 and T_2 , the vertical dashed line shows a crossover at $T \approx J_\perp$, the arrowed lines give schematically the trajectory of relaxation (decrease of the total ν and the cooling).

Before the pumping, at the equilibrium ambient temperature T_{eq} , the solitons are present either as free particles, if $T_{eq} > T_{1eq}$, or as confined pairs if $T_{eq} < T_{1eq}$ where $T_{1eq} = T_1(\nu_{eq}) \propto E_s / \ln(E_s/J_\perp)$ is the ordering transition temperature without pumping. But in any case, the equilibrium concentration of kinks is low: $\nu_{eq} \sim \exp(-E_s/T)$ at $T_{eq} > T_{1eq}$ or $\nu_{bs} \sim \exp(-2E_s/T)$ at $T_{eq} < T_{1eq}$, because now the total big activation energy E_s of the soliton is to be paid in comparison with the relatively small scale of the interchain energy J_\perp when the number of solitons is controlled.

Just after the pumping, the initial concentration of kinks ν_0 is very high and the initial temperature $T_0 > T_{eq}$ is also high (it can even further increase at intermediate times because of the energy release from relaxation of excitations¹⁸). Suppose that $\nu_0 > J_\perp/T_0$ so that we are in the disordered phase above $T_1(\nu_0) \propto J_\perp/\nu_0$ – the pumping has destroyed the long-range order, the solitons are not confined in pairs. With time, both $\nu(t)$ and $T(t)$ decrease, so the two sides of the last inequality move towards each other, the transition is inevitably reached at some time t_1 when $\nu(t_1) = J_\perp/T(t_1)$. Recall that this temperature is well below the thermodynamical transition temperature T_{1eq} since the number of solitons is strongly enhanced.

The situation looks, at first sight, a bit less certain for the lower transition because its expected temperature $T_2(\nu) = J_\perp / \ln(1/\nu)$ falls with decreasing $\nu(t)$, unlike $T_1(\nu)$. But $T_2(\nu)$ decreases very slowly, e.g. $\sim 1/t$ for the exponential decay of ν , that is slower than any expected decrease of $T(t)$. So the second phase transi-

tion will also happen at a certain moment t_2 of time, when $T(t_2) = J_\perp / \ln(1/\nu(t_2))$, then the confined pairs of solitons will start to aggregate into macroscopic domain walls of solitons. The T_2 transition line will be crossed back (via evaporation of domain walls) in the course of returning the temperature to the ambient one and the full annihilation of excess solitons.

III. THE BASIC MODEL.

A. Mapping to the constrained Ising model.

For a generic (no CIs) model, the only configurational energy for the order parameter $\eta_\alpha(x)$ at the point x of the chain α is

$$- \int dx \left(\sum_{\langle \alpha, \beta \rangle} V_\perp \eta_\alpha(x) \eta_\beta(x) + \sum_\alpha U(\eta_\alpha(x)) \right) \quad (1)$$

where V_\perp is the interchain ordering energy density (actually $2ZV_\perp$ is the confinement force F , where $Z = 2, 4$ for $D = 2, 3$) and $U(\eta)$ is a double-shaped potential with two symmetrical minima normalized to ± 1 which determines the possible ground states with no solitons. The soliton is a trajectory, taking the energy cost E_s , which commutes between these two minima; e.g. $\eta(x) = \pm \tanh(x/a)$ or whatever is the antisymmetric solution of the underlying microscopic model. It is convenient to quantize the chain length as $x \Rightarrow x_n = na_\parallel$ in some units a_\parallel well exceeding the intrinsic width a of the soliton (we take a_\parallel to be equal to the quantum zero point limit size l_q – the minimal size of a bisoliton, see section II B) and to introduce the Ising spin variable as $S_{n,\alpha} = \eta_\alpha(x_n)$. Then the solitons, with the density density $c_\alpha(x)$, are seen as sharp kinks, which density is given by the operator $\rho_{n,\alpha}$ such that²⁹

$$\begin{aligned} c_\alpha(x)a_\parallel &= \rho_{n,\alpha} = \frac{1}{2}(1 - S_{n,\alpha}S_{n+1,\alpha}) \\ \langle \rho_{n,\alpha} \rangle &= \nu = N_s a_\parallel / LH^{D-1} \end{aligned} \quad (2)$$

where ν is the mean concentration of solitons per site, N_s is their total number, $L \times H^{D-1}$ are dimensions of the sample. In the single chain limit, S_n and ρ_n play the roles of complementary order and disorder parameters (see e.g.³⁰). The mean density can be controlled by the chemical potential μ_s and we arrive at the Gibbs energy \tilde{H}_0 for the grand canonical ensemble of solitons²⁹

$$\begin{aligned} \tilde{H}_0 &= H_0 + (E_s - \mu_s)N_s = \\ &= -J_\perp \sum_{\langle \alpha, \beta \rangle n} S_{n,\alpha} S_{n,\beta} - J_\parallel \sum_{\alpha, n} (S_{n,\alpha} S_{n+1,\alpha} - 1) \\ J_\perp &= V_\perp a_\parallel, \quad J_\parallel = (E_s - \mu_s)/2 \end{aligned} \quad (3)$$

In a number of cases, particularly in application to doping, the solitons can possess an electric charge. If

screening by the external carriers is strong enough, these solitons behave as neutral ones. However, in case of intermediate or weak screening the charges of solitons must be considered explicitly. Therefore, taking into account the CI, we can add also³¹ the Coulomb energy H_C to the Hamiltonian:

$$\tilde{H} = \tilde{H}_0 + H_C, \quad H_C = \frac{e^2}{2\epsilon} \sum_{n,m;\alpha,\beta} \frac{(\rho_{n,\alpha} - \nu)(\rho_{m,\beta} - \nu)}{|\mathbf{r}_{n,\alpha} - \mathbf{r}_{m,\beta}|} \quad (4)$$

where e is the electron charge and ϵ is the dielectric constant, taken here to be isotropic. It is known that competing short-range attractive and long-range repulsive forces may result in formation of the diverse variety of patterns^{32–35}. In chapter IV we shall describe Monte-Carlo modelling for both neutral and charged cases.

It is remarkable that controlling the chemical potential, the grand canonical ensemble of solitons in a D -dimensional system can be described by the D -dimensional Ising model, while the canonical ensemble is described by the stack of noninteracting $(D-1)$ -dimensional models with an overall constraint. In this anisotropic mode, only the interchain coupling constant J_\perp has a physical origin and is frozen, while the on-chain constant J_\parallel is determined by the chemical potential. Since the physical situations of interest correspond to controlling the concentration ν , then the price, and the source, of most interesting behavior come from the self-consistency condition to invert the function $\nu(\mu, T)$ to $\mu(\nu, T)$, hence traveling over a special line on the surface of Ising model parameters. In this way we can take a good advantage (without CI), of notion on the Ising models (full for $D = 2$ and qualitative at least for $D = 3$). On the other hand, as we shall demonstrate in the following, the numerical procedure can be constructed which allows to directly keep the constraint on the total number of solitons. Then working with the canonical ensemble we get a good advantage to deal with $(D-1)$ -dimensional systems with only physical interchain interaction being present.

B. Estimations based on the effective Ising model for a neutral system

Consider the effective Ising model with variable $J_\parallel = J_\parallel(T, \nu)$ in D dimensions. The concentration of solitons is always supposed to be small $\nu \ll 1$. It is interesting to know what are the adjusted values of $J_\parallel(T, \nu)$.

At $T \gg T_1 \gg J_\perp$, the system is effectively one-dimensional, the energy of one soliton is $2J_\parallel$ and probability to find a soliton at a given point of the dual lattice is $\exp(-2J_\parallel/T) \approx \nu$, then

$$J_\parallel(T, \nu) \approx \frac{T}{2} \ln \frac{1}{\nu} \quad (5)$$

is the effective on-chain coupling, hence, from (3), the solitons' chemical potential increases with decreasing T .

Extrapolating this expression down to T_1 , we find an estimate for T_1 . For $D = 2$ we deduce from Onsager's exact result $\sinh(2J_\perp/T_1) \sinh(2J_\parallel/T_1) = 1$ ³⁶ that $T_1 \sim 2J_\perp/\nu$, which up to a numerical factor, agrees with the result of²⁹ $T_1 \approx 2J_\perp/\pi\nu$ (see also Appendix A). For $D = 3$ we can use the approximation, where the on-chain interaction is treated exactly while the interchain one is taken into account using the mean-field theory. For the critical temperature of anisotropic 3D Ising model this approach gives^{37,38} $T_1 \approx 8J_\perp \exp(2J_\parallel/T_1)$, from which we get $T_1 \sim 8J_\perp/\nu$. We see that both in 2D and 3D the Ising critical temperature behaves as $T_1 \sim J_\perp/\nu$ at $\nu \rightarrow 0$, which justifies treating T_1 as the confinement transition.

Consider now the opposite limit of low temperatures $T \ll J_\perp$. It looks, at first sight and wrongly, that at low temperatures the system persists in a very simple form of one spin-ordered domain impregnated by a dilute gas of spin-reversal points which are our tightly bound bisolitons. Their energy is $2ZJ_\perp$ where $Z = 2, 4$ for $D = 2, 3$ is the number of nearest chain neighbors. Taking into account the chemical potential, their number is (neglecting the excluded volume corrections)

$$\nu_{bs} = \exp\left(-\frac{4J_\parallel + 2ZJ_\perp}{T}\right) \quad (6)$$

Since this number is fixed as $\nu_{bs} = \nu/2$, its decrease with lowering T must be compensated by the decrease of J_\parallel which is limited to be positive $J_\parallel \geq 0$: a negative $J_\parallel < 0$ would switch the system to an "antiferromagnetic" ground state with spins alternation at each site in the chain direction, hence the infinite number of kinks. Hence a new reservoir for the storage of solitons must be opened when T falls below $T_2(\nu)$ such that $\nu = 2 \exp(-2ZJ_\perp/T_2)$ i.e.

$$T_2 \approx \frac{2ZJ_\perp}{\ln(2/\nu)} \quad (7)$$

which agrees with both the estimation (A4) for 2D (with logarithmic accuracy) and with the exact solution (A10) accessible in 3D. This new reservoir can be viewed as a system of stripes (lines in 2D or planes in 3D) which cross the whole sample separating the bulk in noninteracting domains of alternating magnetization. A more thorough analysis²⁹ shows that T_2 must be indeed a sharp phase transition at $D = 3$, while at $D = 2$ T_2 is a crossover for growing rods of a finite extent. Only for a finite 2D system of the width H the rods pass through the entire $L \times H$ sample at $T_F \approx 4J_\perp/\ln(H/2\nu)$.

Estimates for $J_\parallel(T, \nu)$ can also be found at $T \ll J_\perp$. For $D = 2$ as $T \rightarrow 0$ and $D = 3$ as $T \rightarrow T_2 + 0$ we find that $J_\parallel \rightarrow 0$ as (details of derivations are given in the Appendix A):

$$J_\parallel(T, \nu) \propto T \exp(-2J_\perp/T)/\sqrt{\nu} \quad (2D) \quad (8)$$

$$J_\parallel(T, \nu) \propto \nu \ln(1/\nu) \cdot (T - T_2) \quad (3D)$$

Below T_2 in 3D transverse layers do not interact and J_\parallel remains to be 0.

This picture, and its strong complication by long-range CIs will be numerically verified and expanded in the next chapter. Some analytical results for both neutral and charged systems are also given in the Appendices.

IV. NUMERICAL APPROACH

A. Monte Carlo simulation details

In this chapter we consider the Monte Carlo (MC) simulation of the ensemble of solitons. We have studied statistical properties of the canonical ensemble of solitons over broad temperature ranges in two and three dimensions for both neutral and charged solitons.

In the numerical simulations it is more efficient to keep a fixed number of solitons rather than using self-consistent $J_\parallel(T, \nu)$ as we did in the previous section. Then here we shall work with a canonical ensemble of solitons keeping fixed the overall number of solitons, while the number of solitons at a given chain can vary (in contrary to a more restrictive prescription employed in³¹). N_s these two approaches should give convergent results.

The MC simulation was performed with the use of the standard Metropolis algorithm with 3 types of unit movements: moving a single soliton along the chain (Fig.12a), moving a solitons' pair along (Fig.12b) or across the chains (Fig.12c). The type-(b) movement is a superposition of two type-(a) movements, but it is useful to consider the type-(b) movement explicitly since it improves the low-temperature acceptance rate of the algorithm.

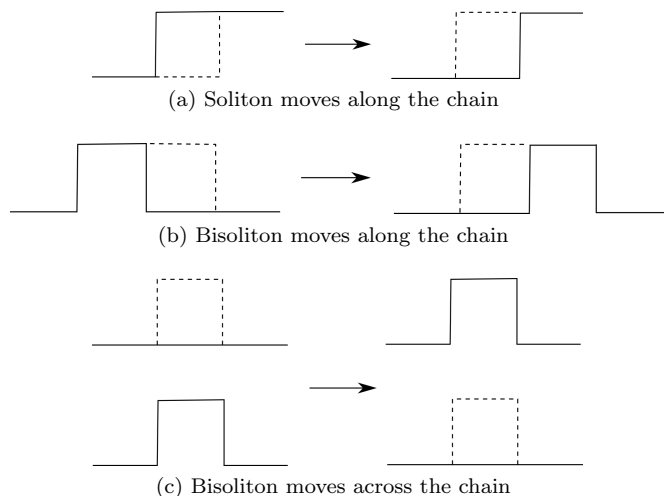


FIG. 5: Three types of elementary MC movements.

For the case of charged solitons, we need to take into account the long-range CI, which is always a formidable task, and even more here for the system prone to patterns formation, owing to appearance of locally non-

compensated charges at a growing scale. Since we are interested in the walls formation process, and for an infinite charged wall the electric potential grows linearly with the distance, then imposing periodic boundary conditions for the Coulomb interactions becomes very important. We use the periodic version of the Coulomb Hamiltonian (4) (for simplicity we put $a_{||} = a_{\perp}$ in the simulation), where the summation goes over not only all pairwise interactions within a computational cell, but also between solitons and their images, between images and with the neutralizing negative background. In practice this is done by technique of Lekner³⁹ for both $2D$ ⁴⁰ and $3D$ ⁴¹ cases. This technique allows to efficiently calculate the force acting on a given particle from another particle and all its images and, by integrating the force, to obtain the effective pairwise potential. Finally, we tabulate this potential for fast computations.

Since the CI is the long-range one, the calculation of the energy change ΔE_C at each MC-step can be time-consuming. To deal with this we use two different approaches. When the MC acceptance rate is high, we employ the first (standard) approach: at each MC trial step we recalculate the CI energy of the shifted soliton with respect to other solitons. However, at low temperatures, when the MC acceptance rate becomes low, it turns out that this approach is ineffective, since many calculations are wasted to compute ΔE_C for rejected steps. Therefore, at low temperatures (and low MC acceptance rates) we use another algorithm^{42,43}: instead of recalculating the interaction energy of the shifted soliton with each other soliton in the system at every trial MC step (computational cost of which is $O(N_s \times N_{trialsteps})$), we introduce an electric potential (ϕ) and use it to calculate the Coulomb energy change: $\Delta E_C \simeq e(\phi(r_{new}) - \phi(r_{old}))$, computational cost of which is only $O(N_{trialsteps})$. However, now we have to update the potential after every successful step at each site of the system, which cost is $O(\text{Volume} \times N_{acceptedsteps})$. This means that this approach works better when the success rate is low. Combining these two approaches allows us to effectively perform simulations for the system with long-range CI at both high and low temperatures and even in $3D$ space.

B. Numerical results for 3D case

In this section we shall describe our main results: evolution of the system with lowering temperature in different regimes. We shall use several presentations: images for distributions of solitons, and of spins. These pictures will be further characterized by plotting the numbers of nearest spins or solitons.

1. Condensation of solitons into walls for neutral solitons

Here we consider a system with the size $50 \times 8 \times 8$ sites and the concentration of neutral solitons $\nu = 0.08$.

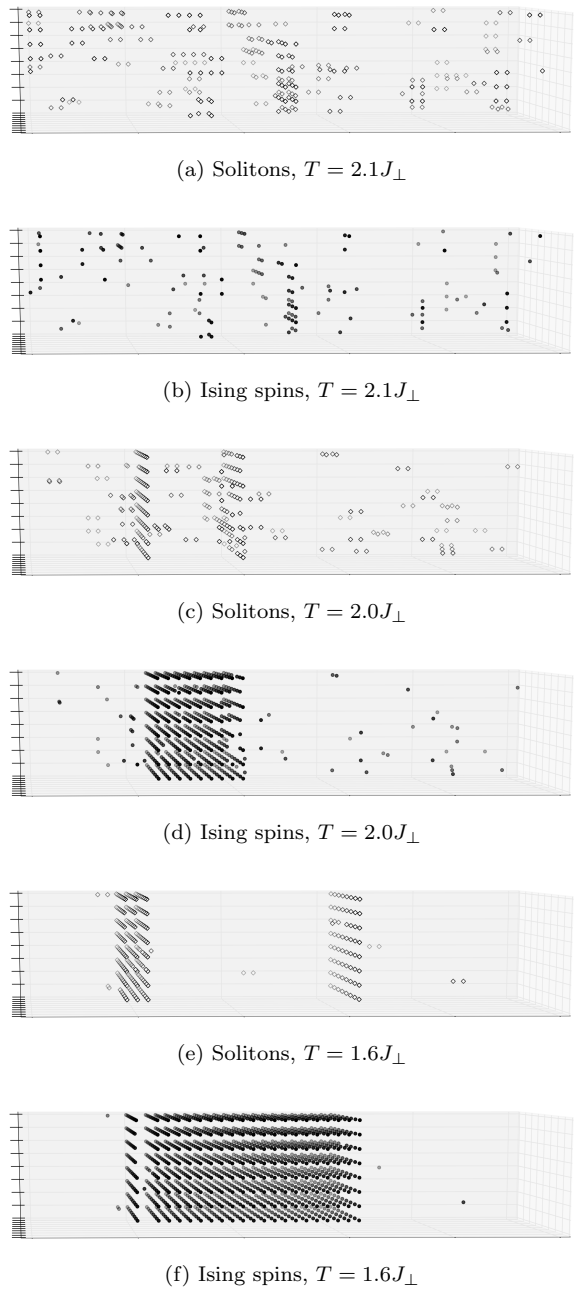


FIG. 6: Process of walls formation in a system $50 \times 8 \times 8$ with $\nu = 0.08$. In Fig. (a),(c),(e) the open circles indicate the positions of solitons. In Fig. (b),(d),(f) the filled circles indicate the positions of the reversed spins. (a,b) $T = 2.1J_{\perp}$, no walls. (c,d) $T = 2.0J_{\perp}$, 2 soliton walls. (e,f) $T = 1.6J_{\perp}$, 4 soliton walls

To demonstrate explicitly the formation and multiplication of domain walls, we shall show the patterns of solitons density (Fig.6a,c,e) which is of our direct interest, and also the patterns of the reversed spins of the effective Ising model (Fig.6b,d,f) which give a useful complementary insight. Here and below, the sites with the major orientation of spins will be left as blank space while the sites with reversed spins will be marked in black. The

edges of black areas in the longitudinal (chains) directions indicate the positions of kinks.

At higher temperatures ($T = 2.1J_{\perp} > T_2$, Fig.6a,b) we observe an ordered state impregnated by a gas of bisolitons. When the first pair of walls condenses (at $T = 2.0J_{\perp} \approx T_2$, Fig.6c,d), the concentration of non-condensed solitons drops, then at lowering the temperature it further decreases gradually, to cure the defects in already existing walls, then it drops sharply again at formation of the next pair of walls ($T = 1.6J_{\perp} < T_2$, Fig.6e,f). Meanwhile, the initial pair of walls diverges losing the mutual correlation and opening the whole domain of reversed spins in between. Comparing distributions of Ising spins and solitons at different temperatures, we see that the number of reversed Ising spins is not conserved (which means that the Ising magnetization can drastically drop below T_2 and take any value between 0 and $1 - \nu$), whereas the number of solitons is preserved.

Interestingly, the second pair of walls nucleates in the vicinity of the first one: the incipient second pair of walls is more stable there. It happens because the movements of solitons intending to build the second wall are prohibited towards the first one, which twice reduces their escape probability, hence promoting the aggregation. For systems with smaller sizes we can perform long enough simulations, when this transient effect vanishes. However, we believe that since our elementary soliton movements are chosen in a natural way, similar to real time soliton dynamics, then such effects can take place in real systems.

2. Integrated characteristics for the neutral system

The obtained patterns and their evolution show up also in integrated characteristics, which may be better accessible to measuring. Thus, we have calculated the temperature dependencies of the Ising spin magnetization and of the number of transverse neighbors. Here we consider 3D systems with sizes $50 \times 8 \times 8$ and $100 \times 20 \times 20$ sites for the concentration of neutral solitons $\nu = 0.08$. Fig.7 shows the magnetization $m(T)$ dependence which is, excluding the low temperature region, very similar to the standard plot for the Ising model with the transition temperature $T_1 \approx 30J_{\perp}$. The transition is smeared due to the finite-size effects.

Apparently, even this not very small fixed concentration of solitons does not affect much the high T properties, unlike the drastic effect we see at low T . The T_2 phase transition happens with the dimensionality reduction of the system. From the thermodynamical point of view, when the interaction between layers vanishes ($J_{\parallel} = 0$), the magnetization must drop to 0. However, the picture is somewhat different if we consider a system in a time evolution. And we believe that since our elementary MC-steps are chosen in a natural way (similar to a real time dynamics), our simulation is consistent with the processes occurring in a real time evolution of

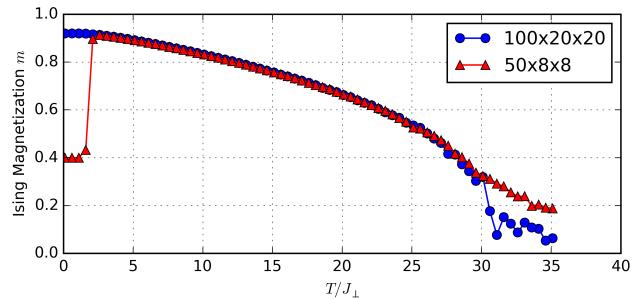


FIG. 7: (Color online) Plot of magnetization m of equivalent Ising spins vs temperature (in units of J_{\perp}) for systems with sizes $100 \times 20 \times 20$ (circles) and $50 \times 8 \times 8$ (triangles), with $\nu = 0.08$.

the system.

For the smaller system $50 \times 8 \times 8$ with lowering temperature we see a sharp drop in the $m(T)$ dependence at $T \approx 2J_{\perp}$. This reflects the walls formation transition at T_2 : as it was explained in section II B and was demonstrated explicitly in section IV B 1, the bisolitons aggregate into walls, then these bisoliton walls divide into single soliton ones and the Ising spins' magnetization drops. Depending on a numerical experiment, m picks a random value between 0 and $1 - \nu$ when the system freezes at $T = 0$. For a sample of a macroscopic length, however, it must be $m(0) = 0$ since spin-up and spin-down domains are equally probable.

For the bigger system $100 \times 20 \times 20$ we have observed that the walls appear in pairs, with only one reversed spin per chain, and a long time is necessary for the walls to diverge, opening a growing domain of reversed spins in between. Typical times of the simulation are not big enough to observe the wall splitting. This happens because in order for the bisoliton wall to divide, the system must pass through an energetically unfavourable state: when the incipient layer of new domain grows to a disk of radius r , the energy increases by $2\pi r \cdot 2J_{\perp}$. If the transverse size H is big enough, this high energy state cannot be reached during the time of the simulation, and the system can not skip from one energy minimum to another with the shifted wall. Therefore for such big systems only bisoliton walls are observed and the Ising magnetization does not decrease at low temperatures.

Since $T_2 \ll T_1$, then in the vicinity of T_2 only a relatively small number of reversed spins is left, being dispersed within the major domain of aligned spins. To characterize the degree of aggregation, we calculate for each reversed Ising spin (or each soliton) the number of its neighboring reversed spins (or neighboring solitons) in the transverse direction respectively. Since for the domain-wall phase the number of bulk spins is much greater than the number of spins at the interfaces, then the number of Ising spin's neighbors must jump to approximately 4 at $T = T_2$. For solitons when T decreases below T_2 a substantial number of solitons condensates

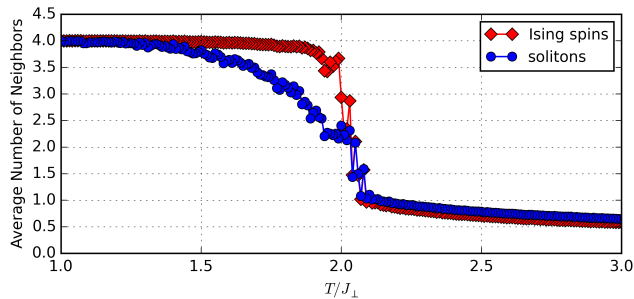


FIG. 8: (Color online) Average number of neighbors vs temperature (in units of J_{\perp}) in a system $50 \times 8 \times 8$ with $\nu = 0.08$. Average number of neighbors for Ising spins is shown with squares, average number of neighbors for solitons is shown with circles.

into walls but this number is comparable with the number of the uncondensed solitons, therefore the jump must be not that big as for the Ising spins.

This reasoning is confirmed by Fig.8, which shows the temperature dependence of average number of neighbors for Ising spins and for solitons. With lowering temperature, at $T \simeq 2.0J_{\perp}$ we see a sudden jump of number of Ising spins' neighbors from ~ 1 to ~ 4 , which indicates the formation of domain walls as it is explicitly confirmed in Fig.6. The observed transition temperature is in the good agreement with the theoretical prediction (7): $T_2 \approx 1.98J_{\perp}$. The corresponding plot for solitons also shows a jump, however not that big: from ~ 1 to ~ 2 average number of neighbors. At $T > T_2$ the two plots are essentially coincide since almost all bisoliton pairs have the minimal size of 1.

3. Intermediate Coulomb interaction

Now we consider the case of electrically charged solitons for a system of $50 \times 8 \times 8$ sites with $\nu = 0.08$. The weak CI (according to estimates, given in the Appendix B) with the Coulomb parameter $V_C = e^2/\epsilon a_{\perp} \lesssim J_{\perp}/H^2$ does not affect the system qualitatively. E.g. for $V_C = 0.01J_{\perp}$ it only lowers the temperature of condensation of solitons into walls by 10% down to $T'_3 \sim 1.8J_{\perp}$.

Therefore, in this section we concentrate on a more interesting case of intermediate values of the Coulomb parameter $J_{\perp}/H^2 \ll V_C \ll J_{\perp}$. In this case the Coulomb interaction is weak enough locally, so it does not prevent the binding of solitons into bisolitons, and even does not destroy the initial correlation of bisolitons at neighboring chains. However, it affects the large-scale structures such as domain walls, since for $V_C \gg J_{\perp}/H^2$ the wall formation becomes energetically unfavorable.

In contrast to the cases of neutral solitons (Fig.8) and weak CI, we do not observe sharp wall's formation transition for the intermediate values of the CI – plot of the average number of neighbors does not show any jumps.

When V_C becomes larger than J_{\perp}/H^2 we still observe bisoliton walls at non-zero temperature, which now have defects (holes). As T goes to 0 these defects are grouping and can cut a wall along one of the transverse directions (Fig.9a).

As V_C further increases, we do not observe walls, but only stripes, which are infinite along one transverse direction and finite along the other (Fig.9b, recall that periodical boundary conditions are imposed). However, it is clear that an infinite system cannot possess such infinite stripes, because they are inefficient in terms of the interchain energy J_{\perp} .

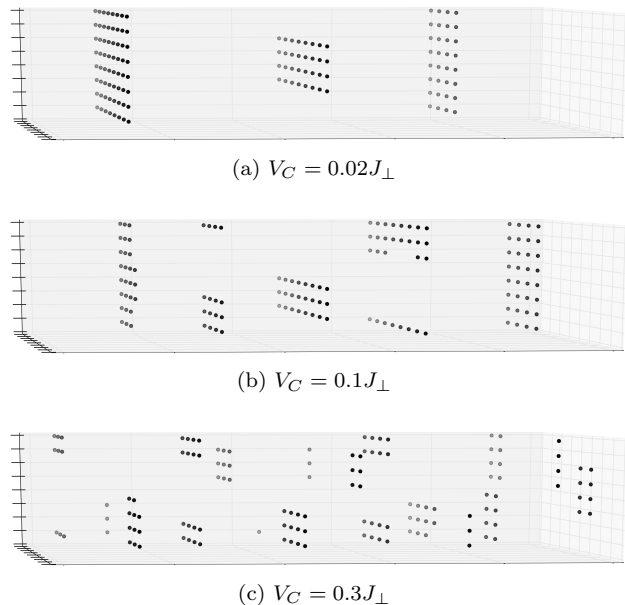


FIG. 9: Disintegration of domain walls as CI increases. Ising spin representation of a system $50 \times 8 \times 8$ with $\nu = 0.08$ at $T = 0.1J_{\perp}$ for different values of the Coulomb parameter. The closed dots indicate the positions of the reversed spins.

Our interpretation for formation of lines rather than planes is that here the system demonstrates an extreme sensitivity of CIs to the transverse finite-size geometry of the sample. A charged wall would create a constant electric field $E = 4\pi e/(\epsilon_{\parallel} a_{\perp}^2)$ in the chains' x direction, which force eE would oppose directly the confinement force J_{\perp} overpassing it at the intermediate CI, hence no stable planes could exist. But forming the stripes (in one transverse y direction) at expense of the part of the confinement energy (lost in the other transverse direction z), the system generates a decreasing electric field $E \propto 1/\sqrt{x^2 + z^2}$ which falls below the confinement force at sufficiently large distances, hence preserving this partial aggregation.

Therefore, in the finite systems the disintegration of plane walls happens via formation of linear structures. For infinite systems we expect that these structures will further disintegrate into finite disks (similar to those we shall see in the next paragraph).

If we choose higher value of the Coulomb parameter,

the formation of "stripes" even for a finite system becomes also energetically unfavorable and we observe only disks of bisolitons (Fig.9c). Observed disk-like formations are consistent with the analytical results presented in Appendix B, where it is shown that the maximum radius of the disks is $R^* \sim \sqrt{J_{\perp}/V_C}$.

4. Strong Coulomb interaction

Here we consider a system of $100 \times 20 \times 20$ sites with $\nu = 0.026$ (parameters were chosen in order to compensate incommensurateness effects, as explained below). Strong CIs $V_C \gtrsim J_{\perp}$ affect the local bisolitons' pairing. The transverse disks shrink to the minimum size of 1 bisoliton. When V_C further increases, these bisolitons form a Wigner "liquid" (Fig.10a) (with a short-range order of individual solitons – in contrary to a Wigner crystal with a long-range order). It is known that the ground state distribution of charges must form a triangular lattice in $2D$ ⁴⁴ and a body-centered cubic lattice in $3D$ ⁴⁵. However, for systems with finite discretization, the commensurateness effects become very important: even small incommensurateness destroys the long-range order, while the short-range order persists⁴⁶.

For even higher V_C , the Coulomb force starts to compete with the confinement force and the size of a bisoliton starts to grow (Fig.10b). Neglecting the interaction between bisolitons we can estimate their size. A bisoliton elongates until the Coulomb force is balanced by the confinement force: $V_C/l_{bs}^2 \sim 8J_{\perp}$, therefore $l_{bs} \sim \sqrt{V_C/8J_{\perp}}$. This estimate holds as long as the average bisoliton size is much less than the distance between them: $l_{bs} \ll \nu_{bs}^{-1/3}$. When $l_{bs} \sim \nu^{-1/3}$ (which happens at $V_C \sim 8J_{\perp}\nu^{-2/3} \sim T_1\nu^{1/3}$) this size becomes comparable to the distance between solitons, interactions between bisolitons become important. Increasing the CI to the highest values, we observe that the Ising order is destroyed in favor of a Wigner "liquid" of individual solitons, rather than bisolitons (Fig.11a,b).

C. Numerical results for the 2D case

1. System of neutral solitons

In this section we consider a $2D$ system with the size of 200×25 sites for concentration of neural solitons $\nu = 0.03$. As discussed in the section IIB, well below the Ising transition temperature T_1 (for the considered system $T_1 \approx 20J_{\perp}$) there exists a characteristic temperature T_2 at which perpendicular rods start to form with their characteristic length gradually increasing with lowering T . For our finite samples, there is also a width H dependent temperature $T_F(H)$ at which these rods become long enough to pass across the entire sample.

Fig.12 shows the Ising spin representation of the system state evolution at lowering T . At a high $T = 10J_{\perp}$

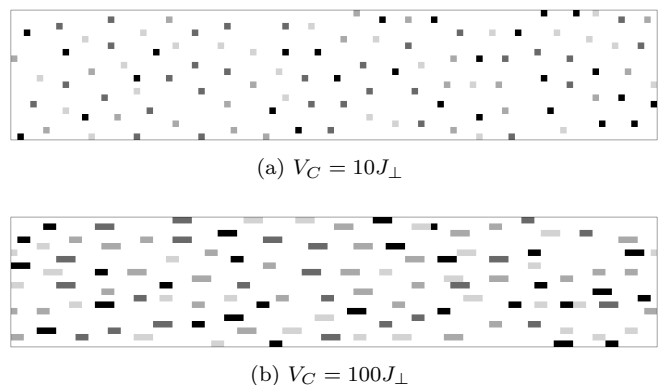


FIG. 10: Ising spin representation of slices $100 \times 20 \times 4$ of a system $100 \times 20 \times 20$, which are projected on the xy -plane, at $T = 0.1J_{\perp}$ for different values of the Coulomb parameter. Reversed spins from four projected planes are marked in different shades of gray. For $V_C = 10J_{\perp}$ (a) we observe a "liquid" of reversed Ising spins (bisolitons at the minimal distance). For $V_C = 100J_{\perp}$ (b) we see that bisolitons' size increases.

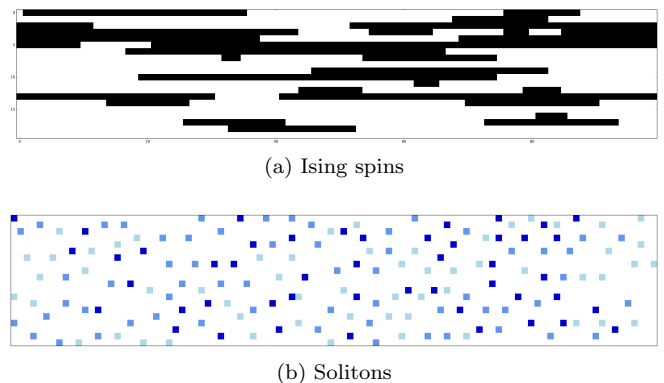


FIG. 11: (Color online) System $100 \times 20 \times 20$ for $V_C = 1000J_{\perp}$, $T = 0.1J_{\perp}$. (a) Ising spin representation of 100×20 slice of the system. The Ising order is destroyed. (b) Soliton representation of $100 \times 20 \times 3$ slice, which is projected on xy plane, solitons from different planes are marked in different shades. The solitons are deconfined, a "liquid" of an individual solitons rather than bisolitons is observed.

(which is still below the Ising transition temperature $T_1 \approx 20J_{\perp}$, Fig.12a) bound pairs of bikinks are observed. These pairs shrink when T lowers (Fig.12b). Then the rods of reversed spins change the predominant orientation from the longitudinal one at high temperatures to the transverse one at low T (Fig.12c). The first case indicate the regime of loosely bound on-chain pairs of kinks, while the second case indicates to the transverse aggregation of tightly bound kinks. Finally, at the lowest considered T (Fig.12d) the aggregated rods cross the entire sample and domains are created.

As in Sec. IV B, T_F lies deeply below the Ising transition temperature, only a relatively small number of reversed spins is left, being dispersed within the major domain of aligned spins; therefore we characterize the de-

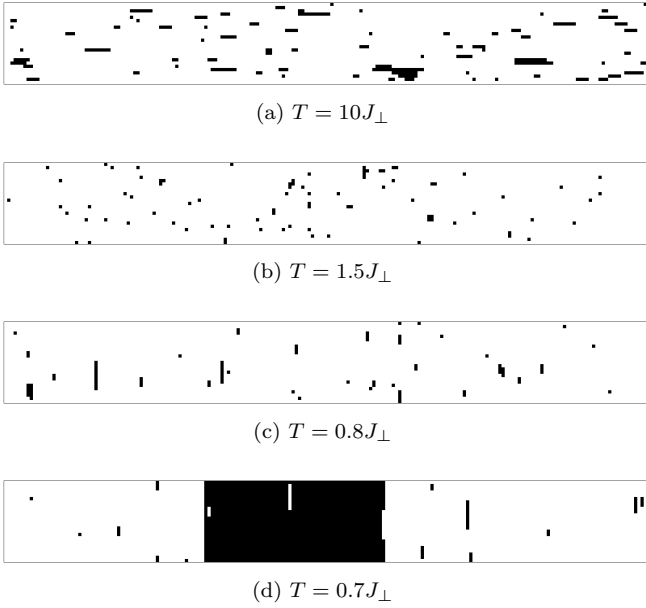


FIG. 12: Neutral solitons: the Ising spins representation of a $2D$ system 200×25 for $\nu = 0.03$ at different temperatures.

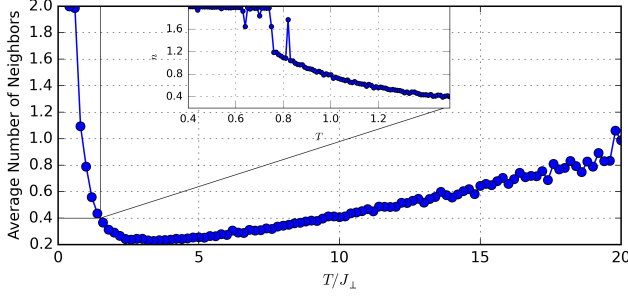


FIG. 13: (Color online) Neutral solitons: average number of Ising neighbors vs temperature in a system of 200×25 sites with $\nu = 0.03$. The inset shows temperature range $T = 0.4J_{\perp} \dots 1.5J_{\perp}$

gree of aggregation, by calculating for each soliton (or each Ising spin) the number of its interchain neighbors. For the domain-wall phase the number of Ising spin's neighbors must be approximately 2.

Fig.13 shows the temperature dependence of the average number of neighbors of the reversed Ising spins. It shows that upon cooling from the Ising transition temperature ($T_1 \approx 20J_{\perp}$) we arrive firstly at some characteristic temperature ($T_2 \approx 2.5J_{\perp}$) when the average number of neighbors starts to grow. On further cooling, another characteristic temperature ($T_F \approx 0.75J_{\perp}$) is reached when the average number of neighbors suddenly changes from ~ 1.2 to ~ 2 which indicates the wall's formation process. Fig.14 shows the temperature dependence of the average number of soliton's interchain neighbors. We see that their number increases gradually with lowering temperature and shows no peculiarities.

This means that the transition at T_F is due to finite-size effects and in an infinite sample we shall observe the condensation of solitons into infinite lines and walls only at $T = 0$.

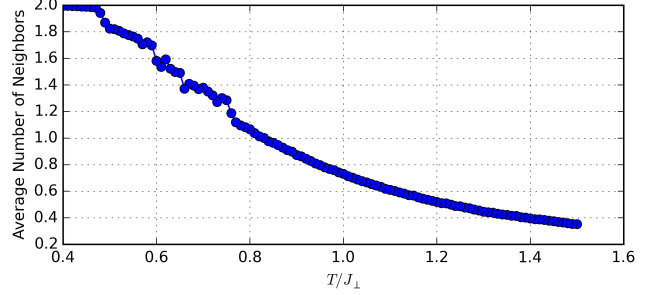


FIG. 14: (Color online) Neutral solitons: average number of solitons' interchain neighbors vs temperature, in a system 200×25 with $\nu = 0.03$.

2. System of charged solitons

Here we consider the similar system, but now the solitons are charged. For $V_C = 0.01J_{\perp}$ (Fig.15a) the temperature T_F is lowered with respect to the case $V_C = 0$ (Fig.13) – now the wall formation transition is observed at the lower $T'_F \approx 0.69J_{\perp}$. Increasing the Coulomb parameter up to $V_C = 0.03J_{\perp}$ (Fig.15) we see that the wall formation transition temperature is further lowered down to $T''_F \approx 0.5J_{\perp}$.

With increasing V_C , T_F eventually decreases to 0. For some critical value of the Coulomb parameter we get $T_F = 0$, in this case rods grow up only to a maximum size $l^* \sim J_{\perp}/V_C \gg 1$ (see Appendix B for the details). However, precise observation of this critical value of V_C is difficult, since the success rate exponentially vanishes to 0 as $T \rightarrow 0$.

For strong CI $V_C \gtrsim 1$, the behavior of the $2D$ system is qualitatively the same as for $3D$. The transverse rods shrink to the minimum size of 1 bisoliton, then the CI start to compete with the confinement force, so bisolitons start to elongate and, at some V_C , the Ising order is destroyed. For the highest values of CIs a Wigner "liquid" of individual solitons is observed.

V. DISCUSSION AND CONCLUSIONS.

We have presented numerical and qualitative analysis of phase transitions in ensembles of solitons as they can be created and studied in experiments on optical pumping and field effect doping in systems with cooperative electronic states.

For $3D$ systems of neutral solitons, as temperature lowers, we observe two phase transitions. The first transition at T_1 reflects the spin ordering of the equivalent Ising

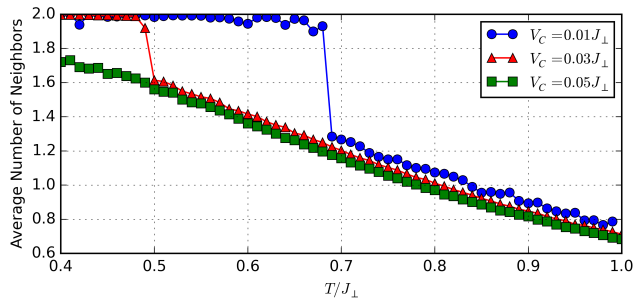


FIG. 15: (Color online) Charged solitons: average number of Ising spins' neighbors vs temperature in a system 200×25 sites with $\nu = 0.03$ for $V_C = 0.01J_\perp$ (circles), $V_C = 0.03J_\perp$ (triangles), and $V_C = 0.05J_\perp$ (squares).

model. In terms of the original solitons, T_1 is the temperature, below which individual solitons become confined into bisoliton pairs. With further lowering temperature, the size of a pair decreases, reaching the minimal value of 1 at $T \sim J_\perp$, the gas of bisolitons forms. At further cooling of the system, the bisolitons start to aggregate into transverse disk-like formations. Finally, at some critical temperature T_2 the second phase transition occurs: these disks cross the entire sample, domain walls are formed and the Ising magnetization drops to 0. The dimensionality of the system effectively reduces to $D = 2$.

For $3D$ systems of charged solitons, the locally small CI (when $V_C \ll J_\perp$) can nevertheless affect the T_2 transition, where macroscopic patterns are created. This happens because a large scale structure, such as a domain wall, gives rise to a high long-range electric field, which erases the gain of the confinement energy reached by the wall formation. For a macroscopic system without an external screening, even an arbitrary small Coulomb parameter $V_C \neq 0$ destroys the walls, only disk-like formations with the maximum size $R^* \propto \sqrt{J_\perp/V_C}$ are observed. However, if the screening is present and the screening length $l_s < R^*$, then these domain walls still cross the entire sample (in our numerical study the sample width H plays a role of the screening length l_s).

For high values of the CI, the disk-like formations disintegrate into separate bisolitons. When the CI is further increased, bisolitons arrange in a Wigner "liquid" state. Further, bisolitons start to elongate and when their size becomes comparable with the interpair distance, the Ising order breaks and a Wigner "liquid" of individual solitons is observed.

Neutral $2D$ systems behave qualitatively similar to $3D$ case at high and intermediate temperatures, the Ising-like transition at T_1 still exists. However, an important distinction is that T_2 is rather a crossover temperature in $2D$: the growing rods do not cross the entire sample for a macroscopic system. But for a finite one, there still exists some temperature T_F of domain walls formation. For charged $2D$ system, T_F lowers with the increase of the CI and, when it reaches 0, only rods of finite transverse

length $l^* \propto J_\perp/V_C$ are observed even at $T = 0$.

The presented results of the MC simulation for neutral solitons agree with the earlier predictions²⁹ (for both $2D$ and $3D$ cases). However, the results for charged solitons do not completely agree with the previous work³¹, performed only for the $2D$ case. There it was observed that with increasing V_C at $T = 0$, domain walls are not destroyed by the CI, but they are rather roughened. This difference in the results occurs presumably because in³¹ the ensemble of solitons was treated with preserving number of bisolitons at each chain, rather than only globally. This limitation is overcome in our treatment which also has employed a more efficient algorithm allowing for modeling of $3D$ systems, even for charged particles. This approach matches the condition of relaxation of solitons' system after a fast optical pumping or an impact of a strong electric field, considered in the present work: only bisolitons can jump between the chains. Actually, there are electron pairs which jump while the order parameter is adjusted to their presence or absence.

For the experiments with optical pumping to the gas of solitons we predict that along the equilibration trajectory the system will experience two phase transitions: confinement of solitons at high T and their aggregation to the stripe phase at lower T . We mention finally that the studied here phase transitions with confinement and with segregation in the ensemble of topologically non-trivial excitations may serve as elementary illustrations to unresolved yet issues in high energy physics (confinement of quarks) and cosmology (phase transitions in the early universe).

Acknowledgements

We acknowledge the financial support of the Ministry of Education and Science of the Russian Federation in the framework of Increase Competitiveness Program of NUST MISiS (No K2-2014-015, No K3-2015-055).

Appendix A: Analytical results for a neutral system

1. $2D$ case

Consider the high temperature regime $T \gtrsim T_1$. The exact expression for the solitons' concentration at the critical temperature is²⁹

$$\nu(T_1, J_\perp) = \frac{1}{2} - \frac{1}{\pi} \cosh \frac{2J_\perp}{T_1} \arctan \frac{1}{\sinh 2J_\perp/T_1}$$

then for the case $\nu \ll 1$ we get

$$T_1 \approx \frac{2J_\perp}{\pi\nu} \quad (\text{A1})$$

Now consider the low temperature regime $T \ll J_\perp$. In this limit all bisoliton pairs are shrunk to the minimal size of one reversed spin, then the magnetization is

$m = 1 - 2\nu_{bs} = 1 - \nu$. Using the exact expression for magnetization in the $2D$ Ising model⁴⁷:

$$m_{2D}(T, J_{\perp}, J_{\parallel}) = \left[1 - \left(\sinh \frac{2J_{\perp}}{T} \sinh \frac{2J_{\parallel}}{T} \right)^{-2} \right]^{1/8} \quad (\text{A2})$$

we find that

$$J_{\parallel}(T, \nu) = \frac{T}{2} \operatorname{arcsinh} \frac{1}{\sinh(2J_{\perp}/T) \sqrt{1 - (1 - \nu)^8}} \approx \frac{T \exp(-2J_{\perp}/T)}{2\sqrt{2\nu}} \quad (\text{A3})$$

Crossover from bikinks' gas state to the state of growing transverse rods occurs when $J_{\parallel}(T, \nu)$ becomes of order of J_{\perp} . Then from (A3) for $\nu \ll 1$ we get with logarithmic accuracy

$$T_2 \approx \frac{4J_{\perp}}{\ln(1/\nu)} \quad (\text{A4})$$

2. 3D case

To find an estimation for $J_{\parallel}(T, \nu)$ at low temperatures $T \ll J_{\perp}$, we employ an approximation where interactions in the transverse planes are considered exactly while the weak interactions between planes are taken into account using the mean field theory.

In this approximation, the in-chain interaction energy terms per spin $S_{n,\alpha}$ becomes

$$-\frac{1}{2} J_{\parallel} S_{n,\alpha} (S_{n+1,\alpha} + S_{n-1,\alpha}) \approx -J_{\parallel} S_{n,\alpha} m = -H S_{n,\alpha} \quad (\text{A5})$$

where H is an effective magnetic field. Therefore the magnetization for $3D$ case is simply given as the magnetization of the $2D$ Ising model in the weak effective magnetic field:

$$m(T) \approx m_{2D}(T) + \chi(T)H \quad (\text{A6})$$

where $\chi(T)$ is the susceptibility of the $2D$ Ising model. Using (A2) and (A6) we get

$$m(T) \approx (1 - (\sinh 2J_{\perp}/T)^{-4})^{1/8} (1 + \chi(T)J_{\parallel}) \quad (\text{A7})$$

Now we link the magnetization m to the solitons' concentration. Since all layers are magnetized in one direction, we introduce deviations from mean magnetization $\delta S_{n,\alpha} = S_{n,\alpha} - m$, so that $\langle S_{n,\alpha} S_{n+1,\alpha} \rangle = m^2 + \langle \delta S_{n,\alpha} \delta S_{n+1,\alpha} \rangle$.

If $T \rightarrow T_2$ then $J_{\parallel} \rightarrow 0$ and $\langle \delta S_{n,\alpha} \delta S_{n+1,\alpha} \rangle \rightarrow 0$, so we can expand the latter in powers of J_{\parallel} :

$$\langle \delta S_{n,\alpha} \delta S_{n+1,\alpha} \rangle = \alpha(T, J_{\perp}) J_{\parallel} + O(J_{\parallel}^2) \quad (\text{A8})$$

Using (2), (A7), (A8) we get:

$$J_{\parallel}(T, J_{\perp}, \nu) = \frac{1 - 2\nu - (1 - \sinh^{-4} \frac{2J_{\perp}}{T})^{1/4}}{2\chi(T, J_{\perp}) (1 - \sinh^{-4} \frac{2J_{\perp}}{T})^{1/4} - \alpha(T, J_{\perp})} \quad (\text{A9})$$

From the condition $J_{\parallel}(T_2, J_{\perp}, \nu) = 0$ we re-derive the result of²⁹:

$$T_2 = \frac{2J_{\perp}}{\operatorname{arcsinh} \left([1 - (1 - 2\nu)^4]^{-1/4} \right)} \approx \frac{8J_{\perp}}{\ln 2/\nu} \quad (\text{A10})$$

To estimate $J_{\parallel}(T, J_{\perp}, \nu)$ we assume that there is no special reasons for the denominator of (A9) being small. So, up to a factor of order of 1, we can neglect α .

For $\chi(T, J_{\perp})$ we use the results of^{48,49}, where it is shown that χ can be decomposed to a well convergent series

$$\chi(T) = \frac{m^2}{T} \sum_{n=1}^{\infty} \hat{\chi}^{(2n)}(T) \quad (\text{A11})$$

$$\hat{\chi}^{(2)} = \frac{(1 + k_{<}^2)E(k_{<}) - (1 - k_{<}^2)K(k_{<})}{3\pi(1 - k_{<})(1 - k_{<}^2)^{3/4}}$$

Here E and K are the complete elliptic integrals of the first and the second kind, $k_{<} = (\sinh 2J_{\parallel}/T \sinh 2J_{\perp}/T)^{-1}$. For $T \ll J_{\perp}$, $k_{<} \approx \exp(-4J_{\perp}/T) \ll 1$, therefore $\hat{\chi}^{(2)} \approx \frac{1}{4}k_{<}^2$, and we estimate χ as:

$$\chi(T, J_{\perp}) \propto \frac{m^2 \exp(-8J_{\perp}/T)}{4T} \propto \frac{\exp(-8J_{\perp}/T)}{4T} \quad (\text{A12})$$

Expanding (A9) in the vicinity of $T = T_2$ and using (A12) we get the desired estimation:

$$J_{\parallel}(T, J_{\perp}, \nu) \propto \frac{64J_{\perp} \exp(-8J_{\perp}/T_2)}{T_2} (T - T_2) \propto 4\nu \ln \frac{2}{\nu} \cdot (T - T_2) \quad (\text{A13})$$

We see that J_{\perp} -dependence is contained only in T_2 and the slope of the line depends only on ν .

Appendix B: Analytical results for a charged system.

Here we present estimations and qualitative arguments on effects of CIs.

1. 2D case.

Consider first the $2D$ case. According to our modelling and following the exact results for the neutral system²⁹, we suggest that the basic units are still the straight lines (rods) of unseparated bikinks; their lengths l will be taken as dimensionless; the physical scale is a_{\perp} .

The CI energy of a line of bikinks is

$$\frac{4e^2}{\epsilon a_{\perp}^2} \int \int \frac{dy dy'}{|y - y'|} \exp\left(-\frac{|y - y'|}{l_s a_{\perp}}\right) \approx 4V_C l \ln \min\{l, l_s\}$$

where $V_C = e^2/\epsilon a_{\perp}$, $l_s a_{\perp}$ is the screening length by remnant or external carries; it appears for $l > l_s$. Our assumption of intermediate CIs is that locally they are weak, i.e. $V_C \ll J_{\perp}$, but become effective for aggregates when $V_C \ln l^*/J_{\perp}$ is not small, i.e. $V_C \gtrsim V_{inter} = J_{\perp}/\ln l^*$ (l^* is the characteristic rods' length).

Because of the equilibrium between rods with respect to exchange of building units – the bikinks, their partial chemical potentials μ_l are related as $\mu_l = 2l\mu^*$; here we include to the definition of $2\mu^*$ not only the soliton energy $2E_s$ but also the CI energy of the elementary pair $e^2/\epsilon a_{\parallel}$, so that $\mu^* = \mu_s - E_s - e^2/2\epsilon a_{\parallel}$. The distribution of segments is

$$n(l) = \exp(-4\beta J_{\perp} + 2\beta\mu^*l - 4\beta V_C l \ln(\min\{l, l_s\}))$$

The parameter $\mu^*(\nu)$ is to be determined from the self-consistency condition

$$\begin{aligned} \nu &= 2 \sum_l n(l)l = \\ &= 2 \exp(-4\beta J_{\perp}) \sum_l l \exp(\beta(2\mu^*l - 4V_C l \ln(\min\{l, l_s\}))) \end{aligned} \quad (\text{B1})$$

Approaching the regime of stripes' formation, the sum is determined by large l , then the summation can be approximated by integration over l .

Consider, first, the case without screening, when the characteristic rods length $l^* \ll l_s$. Now,

$$\nu \exp(4\beta J_{\perp}) = 2 \int dl l \exp(\beta(2\mu^*l - 4V_C l \ln l)) \quad (\text{B2})$$

The exponent $S(l) = \beta(2\mu^*l - 4V_C l \ln l)$ in (B2) is fast decreasing at large l and the integral is convergent, because of the V term, at any – even positive – μ^* . For negative μ^* it decreases rapidly at all l and the sum is saturated already by $n(1) = \exp(\beta(-4J_{\perp} + 2\mu^*))$ with $\nu \approx n(1)$. With decreasing T , μ^* increases, it reaches zero with no qualitative effect unlike the case of neutral systems, and finally becomes positive when $S(l)$ acquires the rising part at $1 < l < l^*$ where the maximum position given by $dS/dl = 0$ is $l^* \approx C \exp(\mu^*/2V_C)$, which makes precise the definition of l^* . The saddle-point approximation for the integral over l gives

$$\begin{aligned} \nu \exp(4\beta J_{\perp}) &\approx 2 \left(\frac{2\pi}{|d^2 S/dl^2|} \right)^{1/2} l^* \exp(S(l^*)) \propto \\ &\propto \left(\frac{T}{V_C} \right)^{1/2} l^{*3/2} \exp(-4J_{\perp}/T) \exp(\tilde{C} V_C l^*/T) \end{aligned}$$

Neglecting pre-exponential numerical coefficients an inversion of this relation to $l^*(\nu)$ and hence to $\mu^*(\nu)$ in the leading dependence for $T \rightarrow 0$ yields

$$\tilde{C} l^* \approx \frac{J_{\perp}}{V_C} + \frac{T}{8V_C} \ln \left(\frac{\nu^2 V_C^4}{T J_{\perp}^3} \right), \quad \mu = 2V_C \ln \frac{J_{\perp}}{V}$$

It yields the saturated value of the rods length $l^*(T \rightarrow 0) = J_{\perp}/V_C$ which is finite but large by our definition of the intermediate CI. The chemical potential saturates at the positive value. This behavior is different from the one in the neutral system in both $D = 2$ and $D = 3$ dimensions. If we now try to find $V_{inter} = J_{\perp}/\ln l^*$, we get an equation $\ln(\tilde{C} \cdot J_{\perp}/V_{inter}) = J_{\perp}/V_{inter}$ which possesses only solutions $J_{\perp}/V_{inter} \sim 1$. This means that if we use l^* as a characteristic length, then there is no intermediate CI regime in $2D$ in the unscreened case.

If the screening is more efficient, such that $l_s < l^*$, then $\ln l$ saturates to $\ln l_s$ and the CIs just shift the chemical potential as $\mu^* \Rightarrow \tilde{\mu} = \mu^* - 2V_C \ln l_s$. Then we get from (3), (A3), (B1)

$$\begin{aligned} \nu &\approx \frac{1}{2} \exp\left(-\frac{4J_{\perp}}{T}\right) \left(\frac{T}{\tilde{\mu}}\right)^2, \quad \tilde{\mu} \approx -\frac{T}{\sqrt{2\nu}} \exp\left(-\frac{2J_{\perp}}{T}\right) < 0 \\ l^* &\approx \frac{T}{2|\tilde{\mu}|} \approx \sqrt{\frac{T}{2\nu}} \exp\left(\frac{2J_{\perp}}{T}\right) > l_s \end{aligned} \quad (\text{B3})$$

which coincides with the appropriate limit of the exact result from²⁹ under the shift $\mu \Rightarrow \tilde{\mu}$. Inversion of this relation gives the chemical potential $\mu^*(\nu, T)$ of individual bisolitons as it is dictated by the reservoir of growing rods. For $T \rightarrow 0$ it saturates at a value $\mu^* \rightarrow 2V_C \ln l_s$ but l^* keeps growing exponentially in $1/T$. In this case the regime of intermediate CIs is determined by l_s : $J_{perp} \gg V \gtrsim V_{inter} = J_{\perp}/\ln l_s$.

In the absence of external carriers, the screening length l_s is defined self-consistently from the contribution of bisolitons and their rods. We shall do it assuming the $3D$ media composed by noninteracting, except sharing the Coulomb potential, layers – that is not the case of our modelling which took a $2D$ layer embedded into the $3D$ space. By definition, the dimensional screening length $a_{\perp} l_s$ is given by the derivative of the the $3D$ charge density $e\nu/(a_{\parallel} a_{\perp}^2)$ over the chemical potential $d\nu/d\mu \approx 4\nu l^*/T$. The last relation follows from differentiation of (B3). We get

$$\begin{aligned} \frac{1}{l_s^2} &= \frac{4\pi(2e)^2}{\epsilon a_{\parallel} a_{\perp}^2} \frac{d\nu/2}{d\mu} \approx 32\pi\nu \frac{V_C}{T} \frac{l^*}{a_{\parallel} a_{\perp}}, \\ \frac{(l^* a_{\perp})^2}{l_s^2} &\approx 32\pi\nu \frac{V_C}{T} \frac{a_{\perp}}{a_{\parallel}} l^{*3} \end{aligned}$$

We see that the condition of the non-screened regime $l^* < l_s$ can be satisfied only for very small ν and still not at very low T . The most common case will be described by relations (B3) which imitates the neutral system but with the up-shifted chemical potentials and the corresponding strong increase of concentration of non-condensed bikinks.

2. 3D case

Consider now the 3D case. Suppose the basic units are the straight bi-discs (lenses) of unseparated bisolitons of radii R (dimensionless; the physical scale is a_\perp).

The CI energy of a disc is

$$\frac{4e^2}{\epsilon a_\perp^4} \iint \frac{d^2r d^2r'}{|\vec{r} - \vec{r}'|} \exp\left(-\frac{|\vec{r} - \vec{r}'|}{a_\perp l_s}\right) \approx 4\pi V_3 R^2 \min\{R, l_s\}$$

where $V_3 = CV_C = Ce^2/\epsilon a_\perp$ with $C = 16/3$ for $R \ll l_s$ and $C = 2\pi$ for $R \gg l_s$. The screening length l_s appears for $R > l_s$. Assumption of intermediate CIs (which are locally weak, but prevent the transverse walls formation) in the 3D case becomes $J_\perp \gg V_3 \gg J_\perp/(H \min\{H, l_s\})$ (the cross-section of the sample is assumed to be $H \times H$ square).

The equilibrium relation for partial chemical potentials is held as before: $\mu_R = 2\pi R^2 \mu$. Then the distribution of disks is

$$n(R) = \exp(\beta(-4\pi R J_\perp + 2\pi R^2 \mu - 4\pi V_3 R^2 \min\{R, l_s\})) \quad (\text{B4})$$

where the first term is the confinement energy lost over the perimeter of the circle. However new items appear in the 3D case, those are domain walls with the chemical potential $\mu_{wall} = \mu H^2$. $\mu(\nu)$ is to be determined from the self-consistency condition

$$\begin{aligned} \nu &= 2 \sum_R \pi R^2 n(l) + H^2 n_{wall} = \\ &= 2\pi \sum_R R^2 \exp(4\pi\beta(R^2 \mu/2 - J_\perp R - V_3 R^2 \min\{R, l_s\})) + \\ &+ H^2 \exp(\beta\mu H^2 - \beta V_3 H^2 \min\{l_s, H\}) \end{aligned} \quad (\text{B5})$$

Even in the case $V_3 = 0$, the wall term does not contribute to the sum as long as $\mu < 0$. But as T decreases, $|\mu|$ has to also decrease in order to accommodate all the solitons in the system. When μ reaches the value $\mu \propto -T/H^2 \approx 0$, the first wall condenses, and then μ stays at 0 analogously to Bose-Einstein condensation, but in the real space instead of the reciprocal one.

First, consider the unscreened case $l_s > H$. Then the summation in (B5) is convergent because of the two terms in the exponent: $J_\perp R$ as it was already without CI, and now also $V_3 R^3$ from the CI. This sum is dominated by the minimal $R \propto 1$ if either $\beta J_\perp \gg 1$ or $\beta V_3 \gg 1$. Recall that our definition of a moderate CI means that it is not efficient at the level of minimal distances, i.e. $J_\perp \gg V_3$, hence only the first inequality is sufficient. Then

$$\nu \approx n(1) \approx \exp(2\beta\mu - 8\beta J_\perp)$$

and the estimation for the transverse aggregation temperature $T_2 \propto J_\perp/\ln(1/\nu)$, obtained for the neutral case, still holds here.

But when the excess number of solitons condenses to first walls, for them R reaches the sample width H . Then

for weak CIs $V_3 \ll J_\perp/H^2$ when it is still unimportant hence qualitatively never important at all. In this case T_2 only slightly decreases by $\Delta T_2 \propto V_3 H^2/\ln(1/\nu)$.

For the moderate CI: $J_\perp \gg V_3 \gg J_\perp/H^2$ walls do not form. We can estimate the maximum size of disks analogously to the 2D case. When T decreases, chemical potential $\mu < 0$ grows, then it reaches $\mu = 0$ and continues to increase. This means that the sum (B5) is now determined by large values of R and summation can be approximated by integration over R .

$$\nu = 2\pi \int dR R^2 \exp(4\pi\beta(R^2 \mu/2 - J_\perp R - V_3 R^3)) \quad (\text{B6})$$

The exponent $S(R) = 4\pi\beta(R^2 \mu/2 - J_\perp R - V_3 R^3)$ in (B6) decreases even faster at large R in comparison to the 2D case, and the integral converges. $S(R)$ has local extrema at points $R_\pm = (\mu \pm \sqrt{\mu^2 - 12V_3 J_\perp})/V_3$ (Fig.16). At some critical value $\mu \geq \mu_{cr} = 4\sqrt{V_3 J_\perp}$ the local maximum becomes positive: $S(R_+) \geq 0$, which means that large disks of radius $R^* = R_+(\mu_{cr}) = \sqrt{J/V_3} \gg 1$ appear in the system. In order to find the corresponding critical $\nu_{cr}(T) = \nu(\mu_{cr}, T)$ we use the saddle-point approximation for the integral over R (only region $R \sim R^*$ contributes in this case)

$$\nu_{cr}(T) \approx 2\pi R^{*2} \left(\frac{2\pi}{|d^2 S/dR^2|} \right)^{1/2} e^{S(R^*)} \approx \pi T^{1/2} J^{3/4} V_3^{-5/4}$$

At $T \rightarrow 0$, $\nu_{cr}(T)$ decreases below the fixed concentration ν , which happens at $T \approx \nu^2 V_3 (V_3/J)^{3/2}$, then the large disks appear.

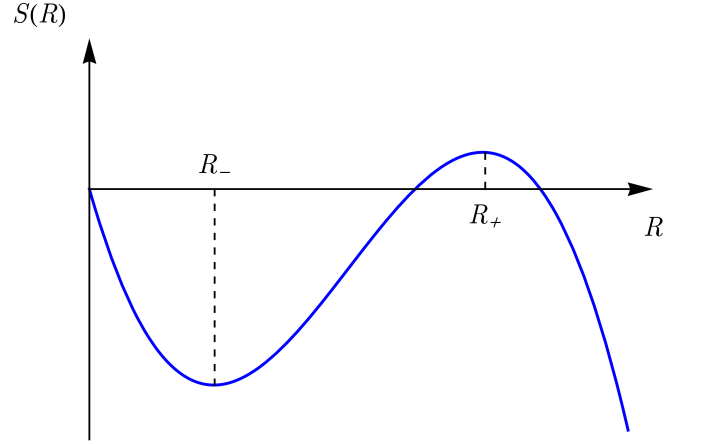


FIG. 16: (Color online) $S(R)$ -dependence and its two local extrema R_\pm .

Now turn to the screened case. For $R^* < l_s < H$, the screening is not very unimportant: it does not affect even the largest disks' structure, but only affects the disk-disk interactions. However, for $l_s < R^*$, the screening becomes important, since disks can grow up to R^* and CIs does not prevent their further growth, so they grow into domain walls. The wall term appears in the sum

(B5) when the chemical potential reaches the value $\mu \approx V_3 l_s$. So, as in the 2D case, at $l_s < R^*$ there is just the shift of the chemical potential $\tilde{\mu} = \mu - V_3 l_s$.

In conclusion, the very weak CI $V_3 \ll J_{\perp}/H^2$ only shifts down the transition temperature T_2 not preventing the formation of the walls. For the intermediate CI $J_{\perp}/H^2 \ll V_3 \ll J_{\perp}$ different regimes are observed de-

pending on the screening length l_s . For $l_s > R^*$ the CI is effectively unscreened, so it prevents the walls' formation and only disks of maximum size of $R^* \approx \sqrt{J_{\perp}/V_3} \gg 1$ are observed. For $l_s < R^*$ the screened CI does not prevent them growing to transverse domain walls and only shifts the chemical potential.

-
- ¹ Photoinduced Phase Transitions, K. Nasu ed., World Scientific, Singapore (2004).
- ² Proceedings of the 4th International Conference on Photoinduced Phase Transitions and Cooperative Phenomena, T. Luty and A. Lewanowicz Eds., Acta Physica Polonica A, **121** (2012).
- ³ 5th International Conference on Photoinduced phase transitions and cooperative phenomena, <http://pipt5.ijs.si/>
- ⁴ C. H. Ahn, A. Bhattacharya, M. Di Ventura, J. N. Eckstein, C. D. Frisbie, M. E. Gershenson, A. M. Goldman, I. H. Inoue, J. Mannhart, A. J. Millis, A. F. Morpurgo, D. Natelson, and J.-M. Triscone, *Rev. Mod. Phys.* **78**, 1185 (2006).
- ⁵ Electronic States and Phases Induced by Electric or Optical Impacts, S. Brazovskii and N. Kirova ed., Eur. Phys. J. Special Topics **222**, #5, (2013)
- ⁶ <http://lptms.u-psud.fr/impact2016/>
- ⁷ S. Brazovskii and N. Kirova, "Electron Selflocalization and superstructures in quasi one-dimensional dielectrics" in *Sov. Sci. Reviews*, v. **A5** edited by I.M. Khalatnikov, Harwood Ac.Publ., NY, p. 99, (1984).
- ⁸ Yu Lu, *Solitons and Polarons in Conducting Polymers*, World Scientific Publ. Co.,NY, (1988).
- ⁹ S. Brazovskii, *J. of Superconductivity and Novel Magnetism*, **20**, 489 (2007); **cond-mat/0709.2296v1**.
- ¹⁰ S. Brazovskii, "Microscopic solitons in correlated electronic systems: theory versus experiment." Advances in Theoretical Physics: Landau Memorial Conference, AIP Conference Proceedings **1134**, 74 (2009).
- ¹¹ S. Brazovskii, *Solid State Sciences* **10**, 1786 (2008); **cond-mat/0801.3202**
- ¹² O. J. Korovyanko, I. I. Gontia, Z. V. Vardeny, T. Masuda, and K. Yoshino, *Phys. Rev. B* **67**, 035114 (2003).
- ¹³ S. Brazovskii and N. Kirova, *JETP Letters* **33**, 4 (1981).
- ¹⁴ I. Gontia, S. V. Frolov, M. Liess, E. Ehrenfreund, Z. V. Vardeny, K. Tada, H. Kajii, R. Hidayat, A. Fujii, K. Yoshino, et al., *Phys. Rev. Lett.*, **82**, 4058 (1999).
- ¹⁵ A. J. Heeger et al., *Rev. Mod. Phys.* **60**, 781 (1988).
- ¹⁶ M. Horvatic, Y. Fagot-Revurat, C. Berthier, G. Dhalenne, and A. Revcolevschi, *Phys. Rev. Lett.* **83**, 420 (1999).
- ¹⁷ F. Kagawa, S. Horiuchi, H. Matsui, R. Kumai, Y. Onose, T. Hasegawa, and Y. Tokura, *Phys. Rev. Lett.* **104**, 227602 (2010), and *rfs. therein*.
- ¹⁸ H. Okamoto, in *Molecular Electronic and Related Materials—Control and Probe with Light*, p. 59, Transworld Research Network (2010).
- ¹⁹ S. Brazovskii, in *Physics of Organic Superconductors and Conductors*, edited by A.G. Lebed, Springer Series in Materials Sciences, **110**, NY, (2008), pp. 313-356; **cond-mat/0606009**.
- ²⁰ S. Brazovskii, Ch. Brun, Zhao-Zhong Wang, and P. Monceau, *Phys. Rev. Lett.* **108**, 096801 (2012).
- ²¹ D. Cho, et al., *Nature Communications*, **7**, 10453 (2016).
- ²² Yu.I. Latyshev, P. Monceau, S. Brazovskii, A.P. Orlov, T. Fournier, *Phys. Rev. Lett.* **95**, 266402 (2005).
- ²³ J. H. Miller Jr., A. I. Wijesinghe, Z. Tang, and A. M. Guloy, *Phys. Rev. B* **87**, 115127 (2013).
- ²⁴ A. Choi et al., *Synthetic Metals* **160**, 1349 (2010).
- ²⁵ N. Kirova, S. Brazovskii, A. Choi, and Y. W. Park, *Physica B: Condensed Matter*, **407**, 1939 (2012).
- ²⁶ A. I. Buzdin and V. V. Tugushev, *Sov. Phys.: JETP* **58**, 428 (1983).
- ²⁷ K. Machida and H. Nakanishi, *Phys. Rev. B* **30**, 122 (1984).
- ²⁸ N. Kirova and S. Brazovskii, *Int. J. of Synthetic Metals*, March 2016, *to be publ.*; arXiv:1512.04282
- ²⁹ T. Bohr, S. Brazovskii, *J. Phys. C: Solid State Phys.* **16**, 1189 (1983).
- ³⁰ A. M. Tsvelik. *Quantum Field Theory in Condensed Matter Physics*. Cambridge University Press (2003).
- ³¹ S. Teber, B. P. Stojkovic, S. Brazovskii, and A. R. Bishop, *J. Phys.: Condens. Matter.* **13**, 4015 (2001).
- ³² C. B. Muratov, *Phys. Rev. E* **66**, 066108 (2002).
- ³³ T. Mertelj, V.V. Kabanov, and D. Mihailovic, *Phys. Rev. Lett.* **94**, 147003 (2005).
- ³⁴ J. Miranda, V.V. Kabanov, *Physica C* **468**, 358 (2008).
- ³⁵ K. Zhang and P. Charbonneau, *Phys. Rev. B* **83**, 214303 (2011).
- ³⁶ L. Onsager, *Phys. Rev.* **65**, 117 (1944).
- ³⁷ T. Graim, D. P. Landau, *Phys. Rev. B* **24**, 5156 (1981).
- ³⁸ D. Hone, P. A. Montano, T. Tonegawa, Y. Imry, *Phys. Rev. B* **12**, 5141 (1975).
- ³⁹ J. Lekner, *Physica A* **176**, 485 (1991).
- ⁴⁰ N. Gronbech-Jensen, G. Hummer and K.M. Beardmore, *Mol. Phys.* **92**, 941 (1997).
- ⁴¹ J. Lekner, *Mol. Phys.* **20**, 357 (1998).
- ⁴² G.S. Grest, *Phys. Rev. B* **39**, 9267 (1989).
- ⁴³ J.-R. Lee and S. Teitel, *Phys. Rev. B* **46**, 3247 (1992).
- ⁴⁴ L. Bonsall and A. A. Maradudin, *Phys. Rev. B* **15**, 1977 (1959).
- ⁴⁵ N. D. Drummond, Z. Radnai, J. R. Trail, M. D. Towler, and R. J. Needs, *Phys. Rev. B* **69**, 085116 (2004).
- ⁴⁶ S. Aubry, *Journal de Physique* **44**, 147 (1983).
- ⁴⁷ B. M. McCoy, T. T. Wu. *The two-dimensional Ising model*. Harvard University Press (1973).
- ⁴⁸ B. G. Nickel, *J. Phys. A: Math. Gen.* **32**, 3889 (1999).
- ⁴⁹ B. G. Nickel, *J. Phys. A: Math. Gen.* **33**, 1693 (2000).